SUPPLEMENTARY INFORMATION

Hepatic stellate cell-derived thrombospondin-2 as a novel therapeutic target for liver fibrosis regardless of etiology

Ning Zhang[1, 2, 5], Xiaoning Wu[1, 2, 5], Wen Zhang[1, 2], Xuzhen Yan[3, 4], Anjian Xu[3, 4], Qi Han[1, 2], Aiting Yang[3, 4], Hong You[1, 2, 6, *], Wei Chen[3, 4, *]

TABLE OF CONTENTS

1. SUPPLEMENTARY EXPERIMENTAL PROCEDURES
2. SUPPLEMENTARY REFERENCES
3. SUPPLEMENTARY FIGURES
4. SUPPLEMENTARY TABLES

SUPPLEMENTARY EXPERIMENTAL PROCEDURES

Reagent and resource. Details of antibodies, chemicals, peptides, recombinant proteins, commercial kits, primary cells/cell lines, organisms/strains, primers for quantitative real time PCR (qPCR), adeno-associated virus serotype 6 (AAV6) vectors, plasmids, short-hairpin RNAs (shRNAs), small interfering RNAs (siRNAs) and software used in this study are summarized in **Table S1**.

Public transcriptomic dataset of liver fibrosis and analysis. Publicly available gene expression profiles of human liver fibrosis were retrieved from Gene Expression Omnibus (GEO) database. A total of 5 transcriptomic profiles (GSE84044 [1], GSE14323 [2], GSE49541 [3], GSE130970 [4], GSE149601) generated from 529 non-fibrotic and fibrotic patients with different etiologies (hepatitis B virus [HBV], hepatitis C virus [HCV], non-alcoholic steatohepatitis [NASH]) were enrolled. *THBS2* gene expression levels detected by microarray or RNA sequencing (RNA-seq) were normalized using the robust multichip average algorithm [5] or scaled into fragments per kilobase per million, respectively. Significance of expression difference of *THBS2* gene was determined by Student's *t* test between groups or one-way ANOVA followed by Tukey's multiple comparisons test among groups. A $p<0.05$ was considered statistically significant. Clinical relevance of *THBS2* gene expression in cirrhosis was evaluated in GSE15654 dataset containing 216 cirrhotic subjects (etiology: HCV) [6]. Sangerbox software (http://sangerbox.com/login.html) was employed to analyze the prognostic values of *THBS2* gene expression in the probability of decompensation occurrence, progression of Child-Pugh class, HCC onset or death. The Log-rank test was used to determine the statistical significance. A $p<0.05$ was considered as statistically significant. Results were visualized using Kaplan-Meier survival curve. Details of these transcriptomic profiles are included in **Table S2**.

Dynamic liver fibrosis mouse model. Liver fibrosis mouse models were established by CCl_4 injection as previously described [7] and bile duct ligation (BDL) operation. Briefly,

to establish chemical damage-induced dynamic liver fibrosis model, collagen α1(I)-GFP mice (eight-week-old, male, kind gift from Prof. David A. Brenner) were intraperitoneally injected of 12.5% CCl_4 (Sinopharm Chemical Reagent Co., Ltd, Beijing, China) in olive oil (1/7, v/v) at a dose of 0.01 ml/g body weight twice a week for 4 weeks (P4) and 12 weeks (P12). After 12-week CCl_4 administration, mice underwent spontaneous recovery for another 4 weeks (R4) after the cessation of CCl_4 injury. Isometric olive oil was injected as control (P0). To build cholestasis-related dynamic liver fibrosis mouse models, C57BL/6J mice (eight-week-old, male) underwent laparotomy and BDL operation. Prior to BDL operation, mice underwent 12 hours of fasting and water deprivation. Post-operative mice were fed normal diet for 7 days (D7) or 14 days (D14). Sham-operated mice (Sham) underwent laparotomy and bile duct mobilization but without BDL operation. All mice were sacrificed at indicated time points; liver and serum were harvested for further analyses. All mice-related studies were approved by the Ethics Committee of Beijing Friendship Hospital, Capital Medical University and performed according to the ARRIVE guidelines.

Cell culture and treatment. Human HSC cell line LX-2 cells (ATCC, NW, USA) and HEK293T cells (ATCC) were cultured in MEM medium (Sigma, MO, USA), supplemented with 10% fetal bovine serum (Sigma). Human primary HSCs (Procell, Wuhan, China) were cultured in special complete culture medium (Procell). All cells were cultured in a humidified cell culture incubator maintained at 37 °C and supplied with 5% CO_2 and 95% O_2. Exponentially growing cells were seeded in 6-well plates or 24-well plates with coverslips (Thermo Fisher Scientific, MA, USA). When cells reaching 80% confluency, THBS2, TLR4, FAK and TGFβ signaling in HSCs were intervened by transfection, infection or co-incubation of human full-length *THBS2* plasmid (pRP[Exp]-EGFP-EF1A>hTHBS2[NM_003247.5]/FLAG, 1-2 μg/mL, 48 hours, Vectorbuilder, Guangzhou, China), human *THBS2* siRNA (si*THBS2*, 20 μM, 48 hours, Hanbio Tech, Shanghai, China), human sh*THBS2* lentiviral particles (LV-sh*THBS2*, 5.0 × 10^7 TU/mL, 72 hours, GeneChem), human THBS2 peptide (0.25-3 μg/mL, 0-24 hours,

Abcam, Shanghai, China), conditioned media from *THBS2* overexpressed LX-2 cells, human full-length *TLR4* plasmid (pRP[Exp]-EGFP-EF1A>FLAG/hTLR4[NM 138554.5], 1-2 μg/mL, 48 hours, Vectorbuilder), TLR4 signaling inhibitor (TAK-242, 1 μM, 24 hours, MCE, Shanghai, China), recombinant human (rh)TGF-β1 (10 μg/mL, 24 hours, R&D Systems, MN, USA), TGFβ signaling inhibitor (LY2157299, 1 μM, 24 hours, MCE), and/or FAK signaling inhibitor (PF-562271, 1 μM, 24 hours, MCE). X-tremeGENE HP DNA Transfection Reagent was used for transfection of plasmids and RNAFit Reagent (HanbioTech, Beijing, China) was used for transfection of siRNAs into LX-2 or HEK293 cells according to the manufacturer's protocols (Roche, Basel, Switzerland).

Serum biochemistry. Serum alanine aminotransferase (ALT) and aspartate aminotransferase (AST) were determined using Alanine aminotransferase Assay Kit (Nanjing Jiancheng, Nanjing, China) and Aspartate aminotransferase Assay Kit (Nanjing Jiancheng) per the protocols. Serum THBS2 levels were quantitated using Mouse Thrombospondin-2 (THBS2) ELISA kit (CUSABIO, Wuhan, China) according to the manufacturer's instruction.

Histological evaluation. Hematoxylin eosin (HE) staining, Sirius Red staining and elastin staining were performed as previously described [7]. HE staining and Sirius Red staining were performed using Hematoxylin-Eosin (HE) Stain Kit and Modified Sirius Red Stain Kit purchased from Solarbio (Beijing, China). Elastic fiber in mouse liver slice was stained using a commercial EVG staining kit (BASO, Wuhan, China) as vendors' protocol. Images of histological staining were captured with a 3Dhistech Panoramic Scanner (3Dhistech, Budapest, Hungary) and semi-quantified using Image-Pro Plus software (Version 6.0, Media Cybernetics, MD, USA).

Quantitative real time-PCR (qPCR). Total RNA was purified using Trizol reagent (Sigma) and reverse transcribed into cDNA using PrimeScript™ RT reagent Kit (Takara Bio, Beijing, China) per manufacturer's protocols. Gene expression was quantified

using an Applied Biosystem 7500 Real-Time PCR System with Fast SYBR Green Master Mix (Applied biosystems, CA, USA) in accordance with the manufacturer's protocols. The mouse *Gapdh* gene was measured and used to normalize the relative abundance of genes. Primers used in our present study were designed by Primer-BLAST webtool.

Western blotting. Whole cell or mouse liver tissue lysates were extracted in ice-cold RIPA lysis buffer (50 mM Tris-HCl pH=8.0, 150 mM NaCl, 5 mM ethylenediaminetetraacetic acid, and 1% NP40) supplemented with a cocktail of proteinase inhibitors (Roche), sonicated, kept on ice for 30 minutes, and centrifuged with 13,500 rpm for 30 minutes at 4°C. Equal amounts of protein (60 μg for liver tissue protein and 30 μg for cell lysate) were subjected to sodium dodecyl sulfate polyacrylamide gel electrophoresis (SDS-PAGE). After transferred onto 0.45 μM nitrocellulose membranes (Millipore, MA, USA) and blocked with 5% non-fat dried milk, blots were incubated overnight at 4°C with indicated primary antibodies, followed by the incubation with appropriate horse radish peroxidase (HRP)-conjugated secondary antibody and the detection using an ECL Plus ChemiDoc Imaging Systems (Bio-Rad, CA, USA). Average relative densitometry values of all bands were analyzed using ImageJ software (NIH) and normalized to GAPDH levels.

Immunohistochemistry. Mouse liver tissues were fixed in 4 % paraformaldehyde, embedded in paraffin and cut into 5-μm slices. Liver slices were deparaffinized in xylene, rehydrated with graded ethanol, immersed in a mixture of 3% hydrogen peroxide (H_2O_2) and 0.3% TritonX-100 for 20 minutes to block endogenous peroxidase activity, and pre-incubated with 10% bovine serum albumin (BSA) to reduce non-specific staining. After that, slices were incubated overnight at 4°C with indicated primary antibody, followed by the incubation of HRP-conjugated secondary antibody for 60 minutes at room temperature. Proteins were visualized by 3,3'-diaminobenzidine tetrahydrochloride (DAB) staining. Images were captured with a 3Dhistech Panoramic

Scanner (3Dhistech) and semi-quantified using Image-Pro Plus software (Version 6.0, Media Cybernetics).

Immunofluorescence. Cells on the coverslips were fixed with ice-cold methanol for 30 minutes. Liver tissues were fixed for 48 hours with 4 % paraformaldehyde, incubated in 20% sucrose before embedding in OCT compound (Sakura, CA, USA), and cut into 7-μm sections. Cell coverslips or liver frozen sections were blocked with donkey serum (Solarbio) for 60 minutes at room temperature after washing three times in PBS. Then, sections were incubated with indicated primary antibodies overnight at 4°C, followed by incubation with Alexa Fluor 488/594 donkey anti-mouse/rabbit secondary antibody (Thermo Fisher Scientific) at dark for 1 hour. Following staining, sections were mounted using 4′,6-diamidino-2-phenylindole (DAPI, Abcam) prior to microscopic visualization by using a laser scanning confocal microscope (Olympus, Tokyo, Japan). Positive staining of interest was semi-quantified using Image-Pro Plus software (Version 6.0, Media Cybernetics).

Ingenuity Pathways Analysis (IPA). Ingenuity Pathway Analysis (IPA) software (QIAGEN, CA, USA) was employed to globally assess the downstream effectors of THBS2 based on the comprehensive, manually curated content of the Ingenuity Knowledge Base.

Co-immunoprecipitation (Co-IP). Co-immunoprecipitation of THBS2 and TLR4 in HEK293T cells after *THBS2* overexpression (1-2 μg/mL, 48 hours) or *TLR4* overexpression (1-2 μg/mL, 48 hours). Cell sediment were lysed in immunoprecipitation lysis buffer (Thermo Fisher scientific). Whole cell lysates were incubated with anti-TLR4 antibody (Thermo Fisher scientific), anti-THBS2 antibody (Santa Cruz, CA, USA) or IgG (negative control) respectively overnight at 4°C. The mixture was incubated and rotated with 80 μL Protein A/G PLUS (Santa Cruz) for 8 hours at 4°C. Afterwards, beads were washed using lysis buffer and boiled with loading

buffer. Immunoprecipitated complexes were analyzed by anti-THBS2 or anti-TLR4 immunoblotting.

Far Western blotting. Extracellular THBS2 ligand-HSC TLR4 receptor interaction was further analyzed using Far Western blotting assay [8]. Briefly, 1 μg of rhTHBS2 protein (ACRO Biosystems), rhTLR4 protein (Abcam) and IgG were used as “prey” proteins and were subjected to SDS-PAGE gel electrophoresis. After transferred onto NC membrane, blots were probed with 500 ng rhTHBS2 (ACRO Biosystems) or rhTLR4 “bait” protein (Abcam) for 2 hours at room temperature. Then, NC membranes were incubated overnight at 4°C with anti-TLR4 antibody (Thermo Fisher Scientific) or anti-THBS2 antibody (Abcam), followed by the incubation with appropriate HRP-conjugated secondary antibody and the detection using an ECL Plus ChemiDoc Imaging Systems (Bio-Rad).

Protein concentration in cell culture medium. Secreted proteins in cell culture media were concentrated using Pierce™ Protein Concentrator PES 10K MWCO, 2-6 mL, 24PK (Thermo Fisher Scientific) strictly as vendors’ protocol.

SUPPLEMENTARY REFERENCES

1. Wang M, *et al.* Characterization of gene expression profiles in HBV-related liver fibrosis patients and identification of ITGBL1 as a key regulator of fibrogenesis. *Sci Rep* **7**, 43446 (2017).

2. Mas VR, *et al.* Genes involved in viral carcinogenesis and tumor initiation in hepatitis C virus-induced hepatocellular carcinoma. *Mol Med* **15**, 85-94 (2009).

3. Moylan CA, *et al.* Hepatic gene expression profiles differentiate presymptomatic patients with mild versus severe nonalcoholic fatty liver disease. *Hepatology* **59**, 471-482 (2014).

4. Hoang SA, *et al.* Gene Expression Predicts Histological Severity and Reveals Distinct Molecular Profiles of Nonalcoholic Fatty Liver Disease. *Sci Rep* **9**, 12541 (2019).

5. Han ES, Wu Y, McCarter R, Nelson JF, Richardson A, Hilsenbeck SG. Reproducibility, sources of variability, pooling, and sample size: important considerations for the design of high-density oligonucleotide array experiments. *J Gerontol A Biol Sci Med Sci* **59**, 306-315 (2004).

6. Hoshida Y, *et al.* Prognostic gene expression signature for patients with hepatitis C-related early-stage cirrhosis. *Gastroenterology* **144**, 1024-1030 (2013).

7. Chen W, *et al.* Dynamics of elastin in liver fibrosis: Accumulates late during progression and degrades slowly in regression. *J Cell Physiol* **234**, 22613-22622 (2019).

8. Wu Y, Li Q, Chen XZ. Detecting protein-protein interactions by Far western blotting. *Nat Protoc* **2**, 3278-3284 (2007).

SUPPLEMENTARY FIGURES

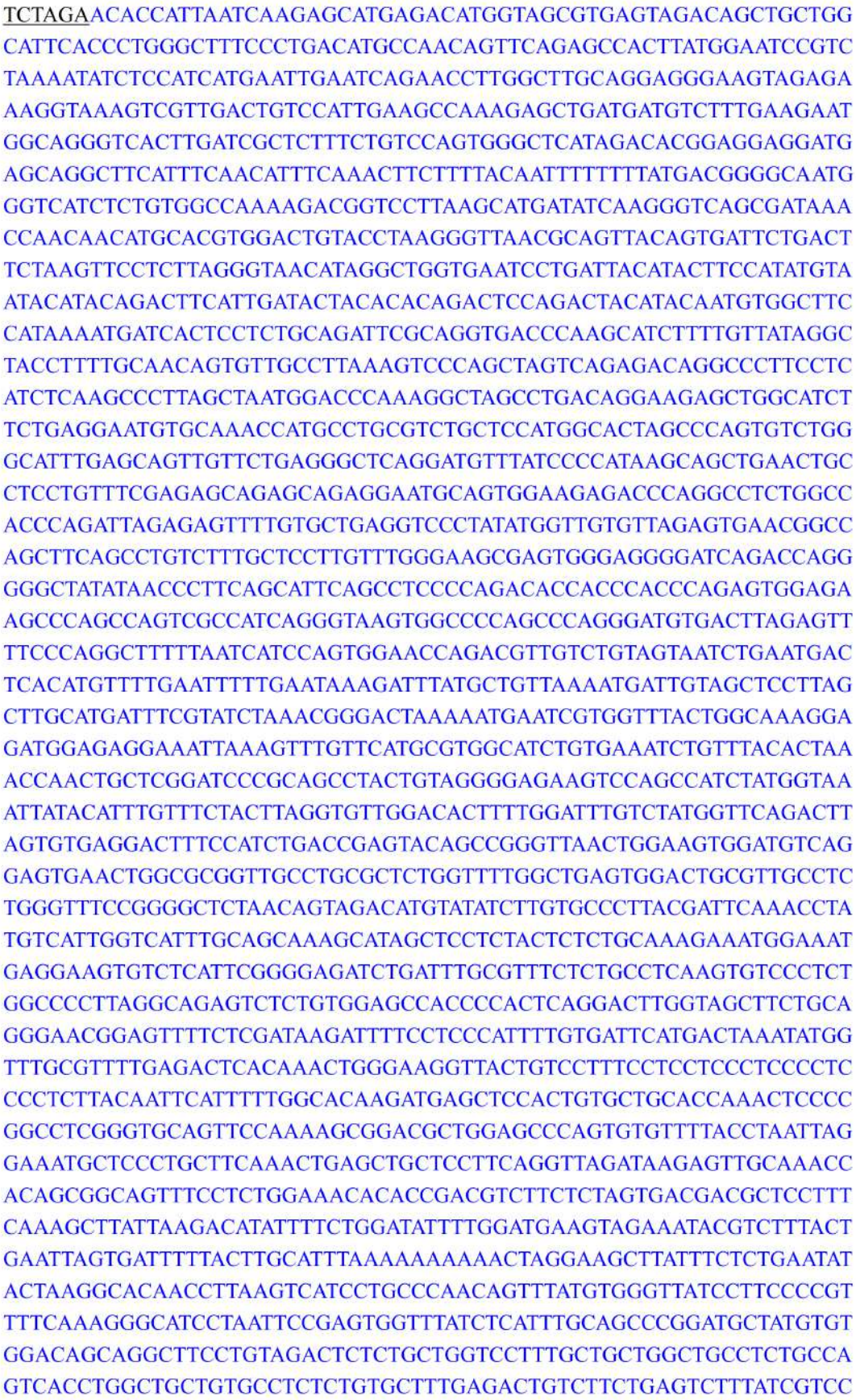

ACTGGAAAGGAAGCTAAATATAATTCAGTGTCTGAAAGAAGAGGCAGAGTAGAGAGA
GGAAAGAGCAAACCAACCAAGATCCCATTATTCCGTTCTTGTGAGGGGAACCCAGGCA
TTGAAGATTTCACTCTGATTTTGGAGGCAGGGTTTGAAAGGAAACCAAAATCACAAAC
AGAATCTCTGGGTAAAGACAATAGTCACATGATGAGATCGACAAGCAATGCTTGTACA
ATGCCCTTGATGTCCCCTGAAGCTGTCGAAAACACAAGCTTAAATGTCAATTACTTAAA
ATGCTATTTTAAGCCCAAAAGAGTATGTGCTCAGTTAGTCAAGGTTAGAAGAAATACCA
GAACTCAGGGAAGAAAAAAAATCTATAAAACCTGATACTTGCCACTTCCAAAGAACCC
CAGTAAATATCTTGGAGAGAATAAGTAAGCTTTGGGGGTGAGGGAGTGGGGGGCAATT
CACATTTTATTACGGTCATATTAAGTTTCTTTCTGTAACTTATCAGTCTTAAGTAAGAATA
GCTATTATCATCCTGTTGGATTTTCAGCTTAGCAGTGATTTTGATTAATGAGGAAATGTT
GTAACTCCTAAAATTGCAAACACCCCCATCAAAAATTTCAATCCAATATTCTCTACTAGA
GTAGCTCTTGCTAGCCTTCAACTTGTGATCCTCCTGCCTCAGCCTCCCAAGTGCTAGGA
TCACAGGTCTACATCACCACGCCCAGTCTTGATTCATGTCTAATGCCTCACCAGCACAA
AAGTCTTCAGAGACAAAAGATTTTTCTTTTAAACATTTAATATGAGCAAACATTTTAAC
ATTTTCACATTCTCATATGCTGCCCATTATTCAAAAATCTACCTTTTTGGGGAAAAATATA
TTTTACAAAAAAAAAAGTGAGTTTGGTTTGATATAGATAACAAACAAAACTAGATAGTT
CTTTAACATGTGCTAATCACTATGTCCCTATAGACCTGTGTTCTCCACTCAGGACCTCTC
ATCTGTGCTCTGTGGCCTGTTCACACACTAATGCTCTGCCCTGCTTGAGAGTGTTAAAA
GAGCCTGTGACGCTCCTGCTCTTTGTGCTGAGGGCTTGTGGTGCTAACCTGGAAGTCA
GGGTTTCAGCTCATCAAAGGCTTTACAGCCTGGTGAAAGCATTTCAAGATAAAGAGTG
TTAGTTGAGATCTGGGGAGAGAACACAACAGGGCCAAGAACCCTGGTTGTGGTTGGG
AGTGACCGTAGGCTCCAGCCAAACGCTCTACATTGCAGTAGCTGCTCCCTCTGTCTCTG
CAGAACCTCGAGAAGCTGCTCCAGCTACCGGTCGCCACCATGGTGAGCAAGGGCGAG
GAGCTGTTCACCGGGGTGGTGCCCATCCTGGTCGAGCTGGACGGCGACGTAAACGGC
CACAAGTTCAGCGTGTCCGGCGAGGGCGAGGGCGATGCCACCTACGGCAAGCTGACC
CTGAAGTTCATCTGCACCACCGGCAAGCTGCCCGTGCCCTGGCCCACCCTCGTGACCA
CCCTGACCTACGGCGTGCAGTGCTTCAGCCGCTACCCCGACCACATGAAGCAGCACGA
CTTCTTCAAGTCCGCCATGCCCGAAGGCTACGTCCAGGAGCGCACCATCTTCTTCAAG
GACGACGGCAACTACAAGACCCGCGCCGAGGTGAAGTTCGAGGGCGACACCCTGGTG
AACCGCATCGAGCTGAAGGGCATCGACTTCAAGGAGGACGGCAACATCCTGGGGCAC
AAGCTGGAGTACAACTACAACAGCCACAACGTCTATATCATGGCCGACAAGCAGAAGA
ACGGCATCAAGGTGAACTTCAAGATCCGCCACAACATCGAGGACGGCAGCGTGCAGC
TCGCCGACCACTACCAGCAGAACACCCCCATCGGCGACGGCCCCGTGCTGCTGCCCGA
CAACCACTACCTGAGCACCCAGTCCGCCCTGAGCAAAGACCCCAACGAGAAGCGCGA
TCACATGGTCCTGCTGGAGTTCGTGACCGCCGCCGGGATCACTCTCGGCATGGACGAG
CTGTACAAGTAAGGTACCCTGGAGGCTTGCTGAAGGCTGTATGCTGACGTGACACGTT
CGGAGAAGTTTTGGCCACTGACTGACTTCTCCGAGTGTCACGTCAGGACACAAGGCC
TGTTACTAGCACTCACATGGAACAAATGGCCCCGGCAATAAAAAGACAGAATAAAACG
CACGGGTGTTGGGTCGTTTGTTCCACGTG

Figure S1. Sequence of αSMA (promoter)-EGFP-MIR155 backbone. Sequences of αSMA promoter (blue), EGFP (green) and MIR155 backbone (red) are color-coded. TGTAGA at the beginning represents *XbaI* site and CACGTG at the last represents *PmlI* site.

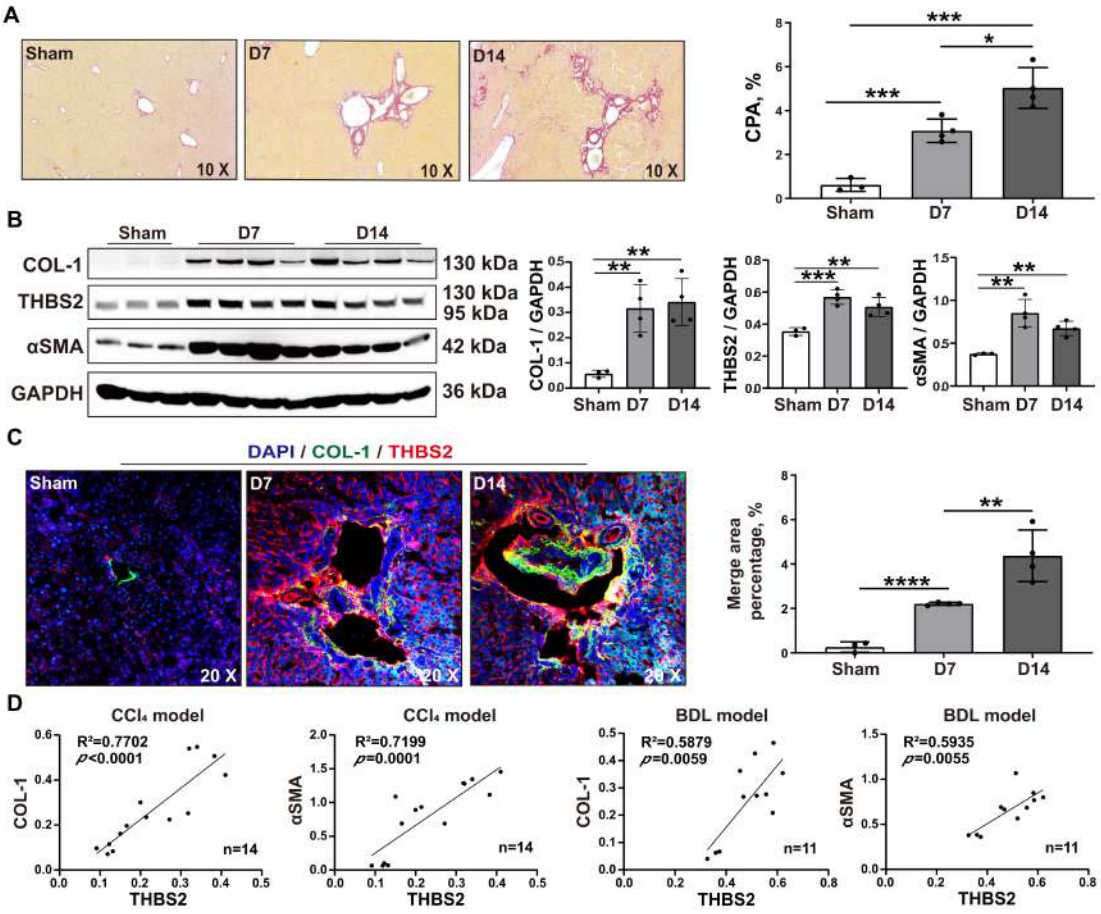

Figure S2. HSC THBS2 protein was upregulated in BDL-induced dynamic liver fibrosis mouse models. (**A**) Sirius red staining of liver slices from BDL-induced dynamic liver fibrosis mouse models. Collagen proportionate area (CPA) is compared among groups. Sham, sham operation (n=3); D7, 7 days after BDL operation (n=4); D14, 14 days after BDL operation (n=4). (**B**) Immunoblotting analyses of liver collagen I, THBS2 and αSMA in Sham, D7 and D14 mice. (**C**) Co-localization (yellow) of THBS2 (red) and collagen I (green) in liver slices from Sham, D7 and D14 mice (objective magnification, 20X). Co-localized area (yellow) percentage is calculated and compared among groups. (**D**) Expression correlation analyses of THBS2 with collagen I or αSMA in both dynamic CCl_4 or BDL-induced mouse models. *p<0.05, **p<0.01, ***p<0.001, ****p<0.0001.

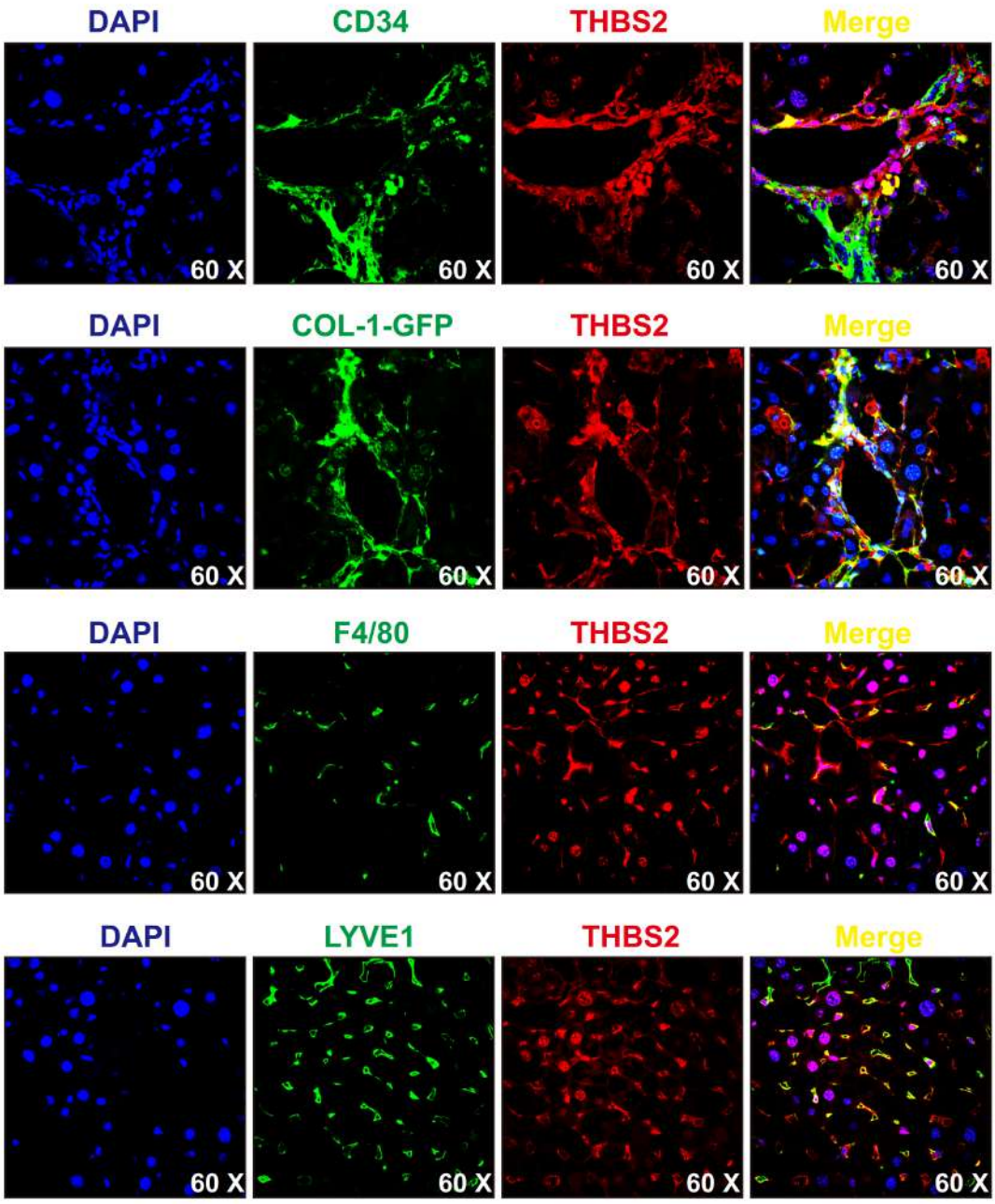

Figure S3. Analysis of cellular source for THBS2 expression in liver. Immunofluorescent staining of THBS2 (red), CD34 (green), COL-1-GFP (autofluorescence, green), F4/80 (green) and LYVE1 (green) in liver slices from CCl_4-induced liver fibrosis mice (P12). The merged area is shown as yellow (objective magnification, 60X).

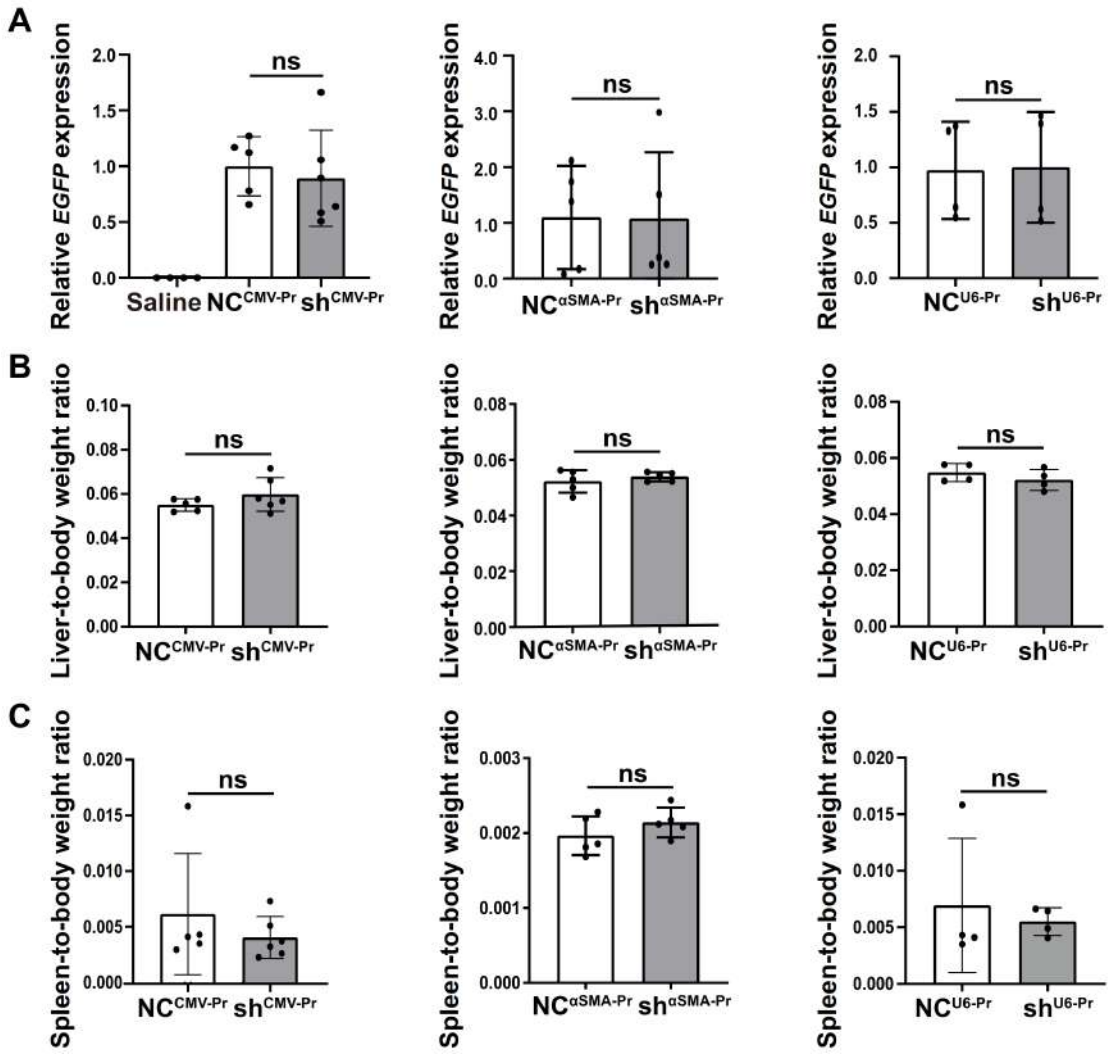

Figure S4. Measurement of *EGFP* mRNA, liver-to-body weight ratio, and spleen-to-body weight ratio in each group of mice. Comparisons of (**A**) *EGFP* mRNA expression, (**B**) liver-to-body weight ratio, and (**C**) spleen-to-body weight ratio among saline, $NC^{CMV\text{-}Pr}$ and $sh^{CMV\text{-}Pr}$ mice, and between $NC^{\alpha SMA\text{-}Pr}$ and $sh^{\alpha SMA\text{-}Pr}$ mice, and between $NC^{\alpha SMA\text{-}Pr}$ and $sh^{\alpha SMA\text{-}Pr}$ mice. ns represents no change.

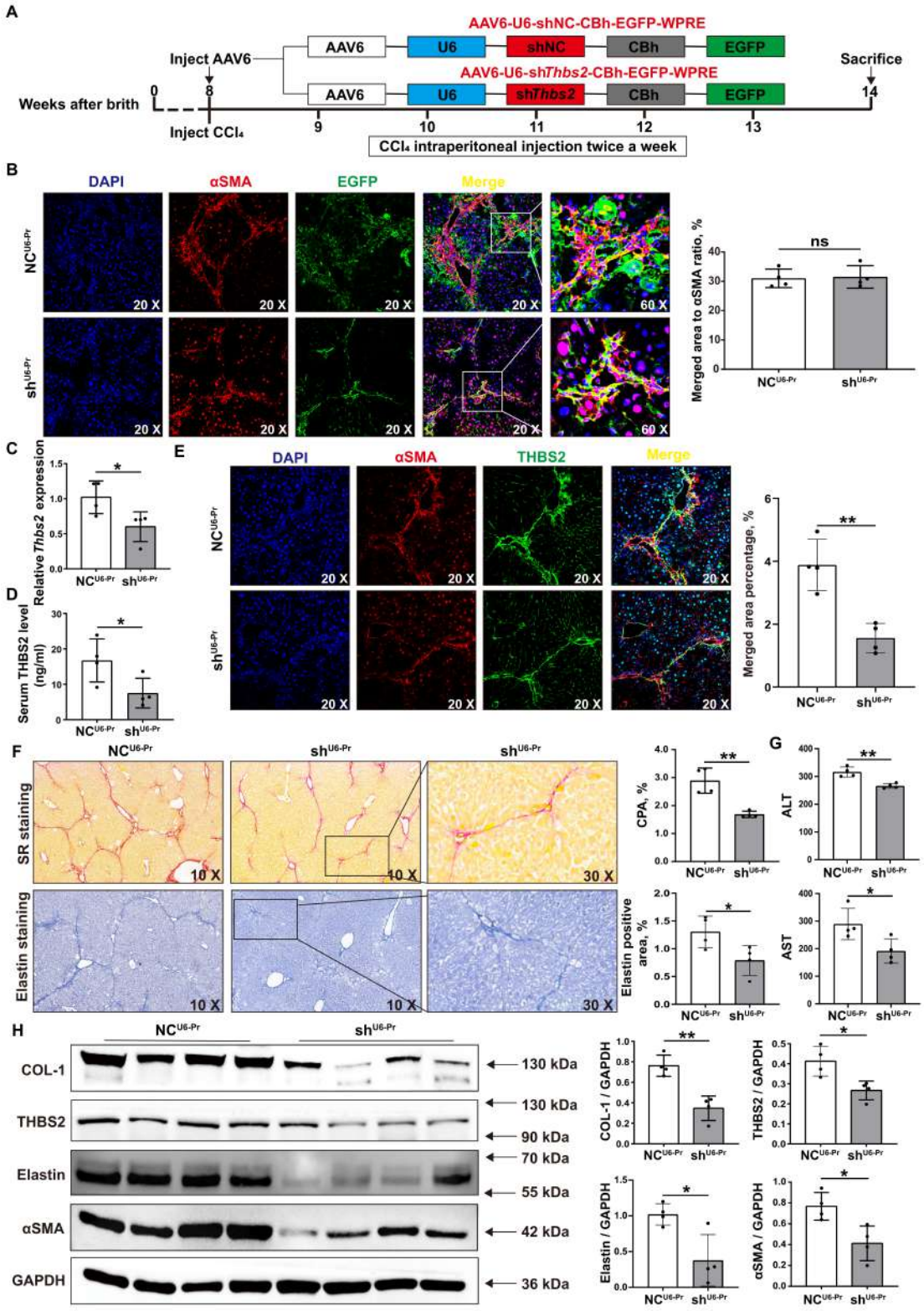

Figure S5. Silence of *Thbs2* in HSCs by AAV6-U6-sh*Thbs2*-CBh-EGFP vector inhibits CCl_4-induced liver fibrosis aggravation in mice. (**A**) Schematic diagram of time points for AAV6 vector injection, CCl_4 administration and sacrifice of mice. (**B**) Immunofluorescent staining of EGFP and αSMA in liver slices from $NC^{U6\text{-}Pr}$ (AAV6-U6-

NC-CBh-EGFP) and $sh^{U6\text{-}Pr}$ (AAV6-U6-sh*Thbs2*-CBh-EGFP) mice (objective magnification, 20X and 60X). Co-localization of EGFP (green) and αSMA (red) is shown as yellow. Merged area (yellow) to αSMA (red) ratio is calculated and compared between groups. (**C**) Comparison of liver *Thbs2* gene expressions between $NC^{U6\text{-}Pr}$ and $sh^{U6\text{-}Pr}$ mice. (**D**) Comparison of serum THBS2 levels between $NC^{U6\text{-}Pr}$ and $sh^{U6\text{-}Pr}$ mice. (**E**) Co-localization (yellow) of THBS2 (green) and αSMA (red) in liver slices from $NC^{U6\text{-}Pr}$ and $sh^{U6\text{-}Pr}$ mice (objective magnification, 20X). Merged area (yellow) percentage is compared between groups. (**F**) Sirius red (SR) staining and elastin staining of liver slices from $NC^{U6\text{-}Pr}$ and $sh^{U6\text{-}Pr}$ mice (objective magnification, 10X and 30X). Collagen proportionate area (CPA) or elastin positive area is compared between two groups. (**G**) Serum ALT and AST levels between $NC^{U6\text{-}Pr}$ and $sh^{U6\text{-}Pr}$ mice. (**H**) Immunoblotting analyses of liver collagen I (COL-1), THBS2, elastin (tropoelastin) and αSMA proteins in $NC^{U6\text{-}Pr}$ and $sh^{U6\text{-}Pr}$ mice. *p<0.05, **p<0.01, ns represents no change; n=4 for each group.

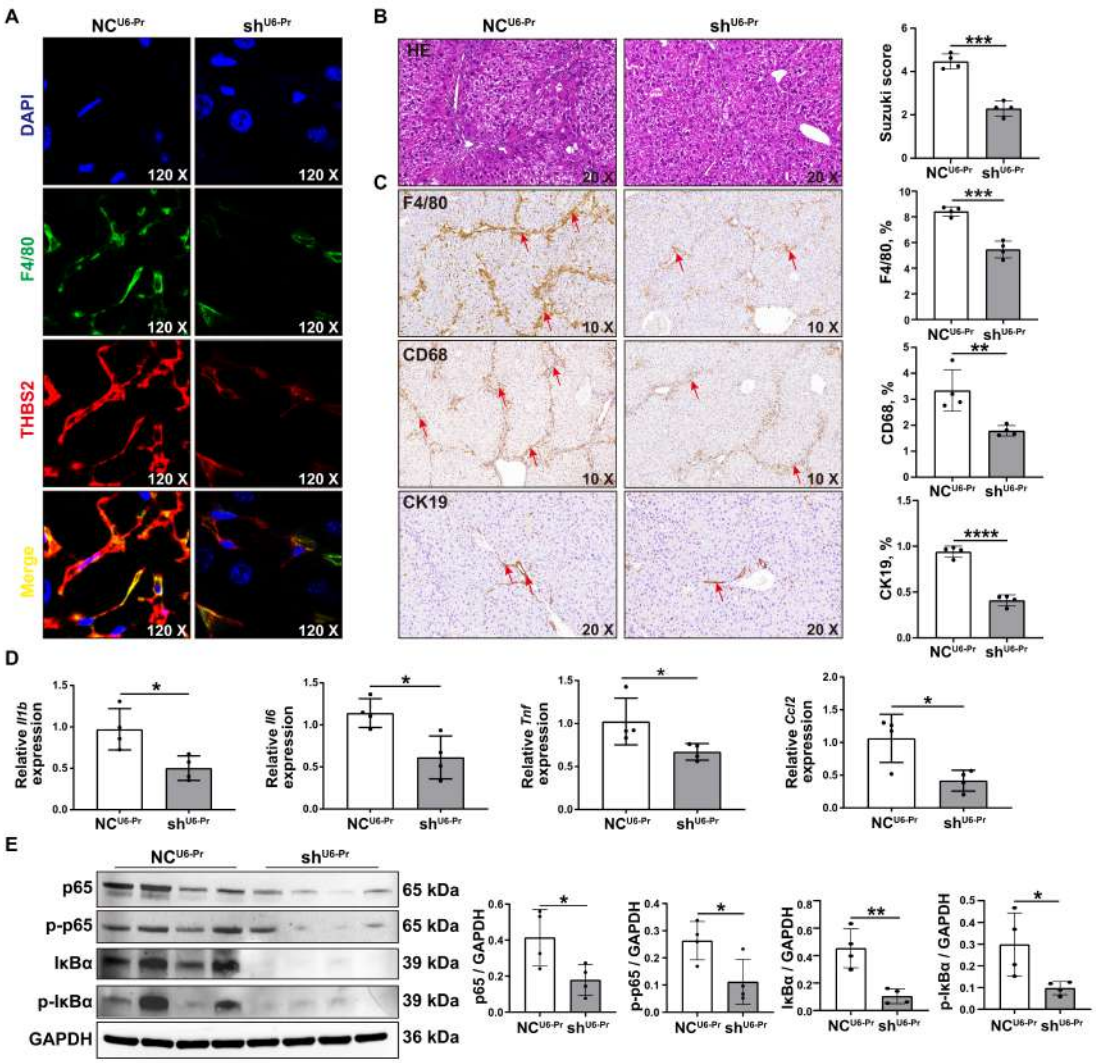

Figure S6. AAV6-U6-sh*Thbs2*-CBh-EGFP vector injection reduces intrahepatic inflammation in CCl_4 mouse models. (**A**) Co-localization (yellow) of F4/80 (green) and THBS2 (red) in liver slices from $NC^{U6\text{-}Pr}$ and $sh^{U6\text{-}Pr}$ mice (objective magnification, 120X). (**B**) HE staining of liver slices from $NC^{U6\text{-}Pr}$ and $sh^{U6\text{-}Pr}$ mice and comparison of Suzuki scores (objective magnification, 20X). (**C**) Immunohistochemical staining of F4/80, CD68 and CK19 in liver slices from $NC^{U6\text{-}Pr}$ and $sh^{U6\text{-}Pr}$ mice and comparison of positive areas (objective magnification, 10X and 20X). Positive staining is marked by arrow. (**D**) Liver proinflammatory gene expression (*Il1b*, *Il6*, *Tnf* and *Ccl2*) measurement and comparison between $NC^{U6\text{-}Pr}$ and $sh^{U6\text{-}Pr}$ mice. (**E**) Immunoblotting analyses of liver p65, phosphorylated (p)-p65, IκBα and phosphorylated (p)-IκBα in $NC^{U6\text{-}Pr}$ and $sh^{U6\text{-}Pr}$ mice. *p<0.05, **p<0.01, ***p<0.001, ****p<0.0001; n=4 for each group.

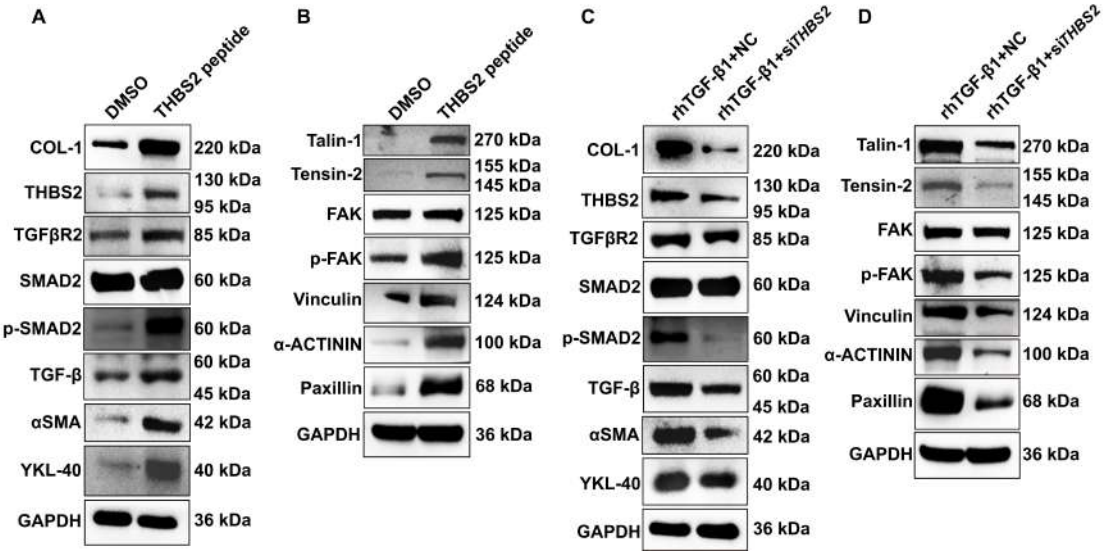

Figure S7. Effects of THBS2 on TGF-β/FAK signaling axis and HSC activation. (**A-B**) Immunoblotting analyses of TGF-β signaling biomarkers (TGFβR2, SMAD2, p-SMAD2, TGF-β, and YKL-40), FAK signaling biomarkers (Talin-1, Tensin-2, FAK, p-FAK, Vinculin, α-Actinin, and Paxillin), HSC activation biomarkers (COL-1 and αSMA), and THBS2 expression in LX-2 cells after THBS2 peptide treatment (1 μg/mL, 24 hours). (**C-D**) Immunoblotting analyses of TGF-β signaling biomarkers, FAK signaling biomarkers, HSC activation biomarkers, and THBS2 expression in LX-2 cells after si*THBS2* treatment (20 μM, 48 hours) under the pressure of rhTGF-β1 incubation (10 μg/mL, 24 hours).

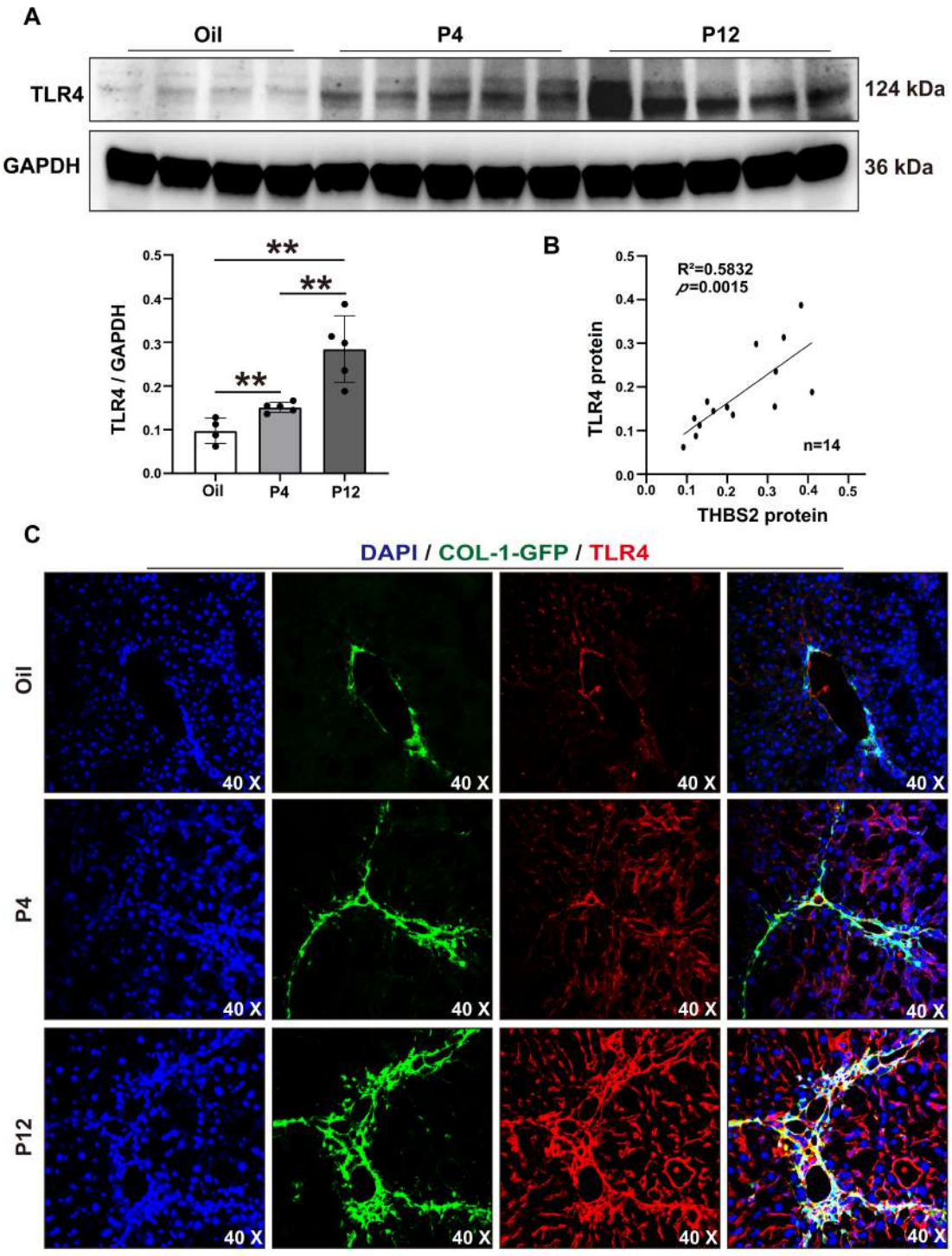

Figure S8. HSC TLR4 expression is increased along with liver fibrosis progression. (**A**) Immunoblotting analyses of liver TLR4 protein in liver fibrosis progressive mouse models injured by CCl_4. Oil, olive oil (n=4); P4 or P12, CCl_4 intoxication for 4 or 12 weeks (n=5). (**B**) Expression correlation analysis of TLR4 and THBS2 protein in dynamic liver fibrosis mouse models induced by CCl_4 (n=14). (**C**)

Immunofluorescent staining of TLR4 and visualization of COL-1-GFP in mouse fibrotic liver slices (objective magnification, 40X). Co-localization of COL-1-GFP (green) and THBS2 (red) is illustrated by the yellow color in the merged images. ** $p<0.01$.

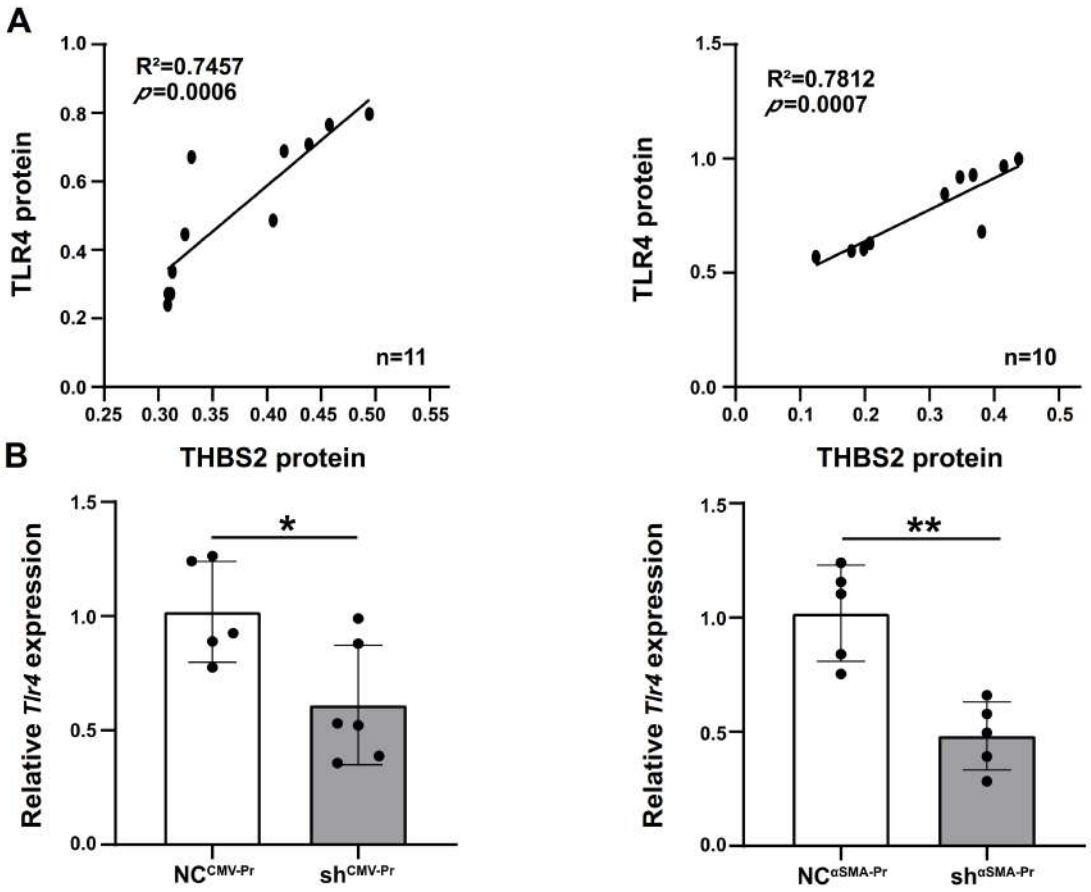

Figure S9. TLR4 expression is closely correlated with THBS2. (**A**) Expression correlation analysis of TLR4 and THBS2 protein in $NC^{CMV\text{-}Pr}$ and $sh^{CMV\text{-}Pr}$ mice (n=11), and $NC^{\alpha SMA\text{-}Pr}$ and $sh^{\alpha SMA\text{-}Pr}$ mice (n=10). (**B**) Gene expression change of liver *Tlr4* in response to AAV6-sh*Thbs2* delivery under the control of CMV or αSMA promoter. **p*<0.05, ***p*<0.01.

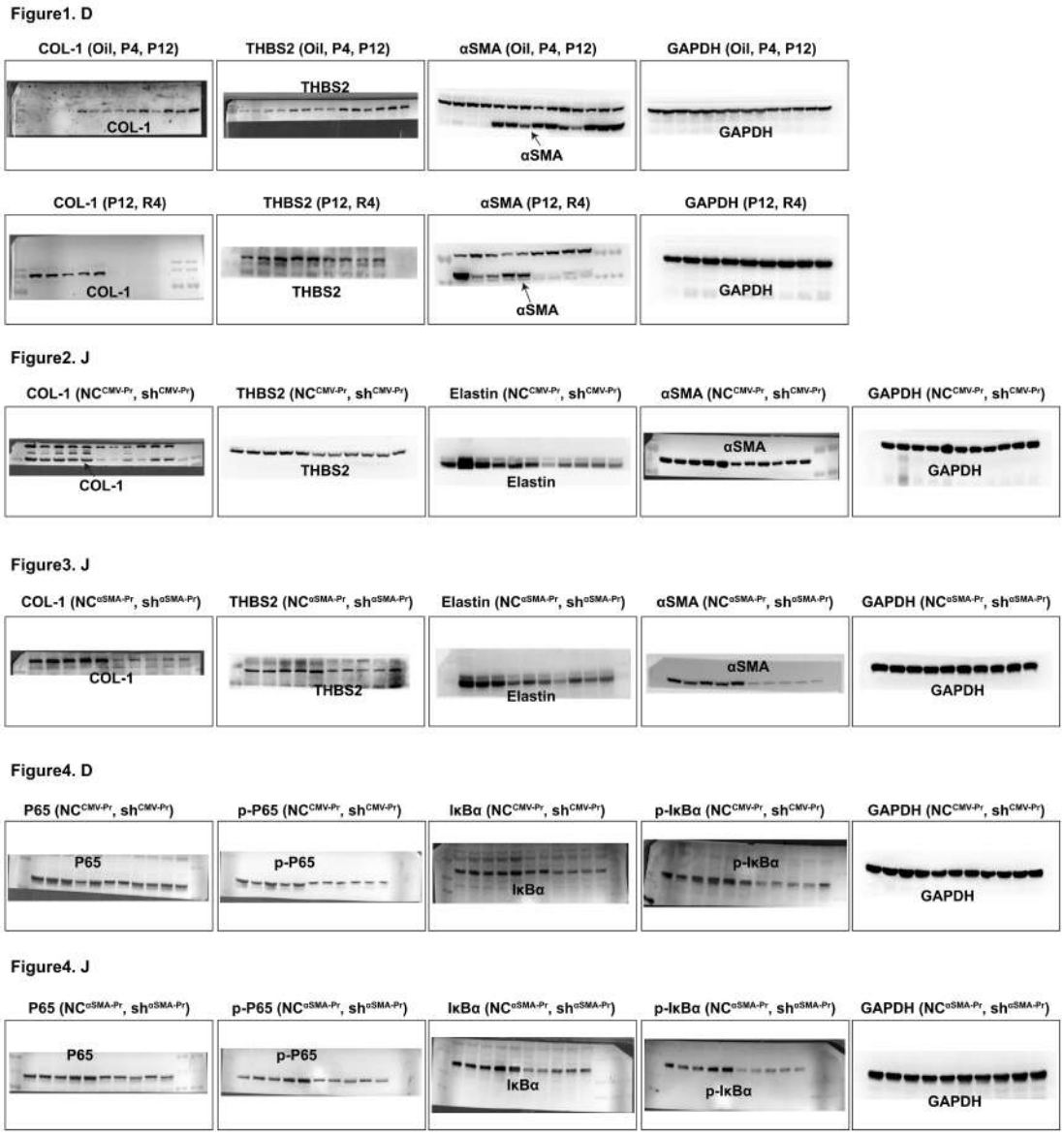

Figure S10. Full-length immunoblots related to Figure 1D, 2J, 3J, 4D and 4J.

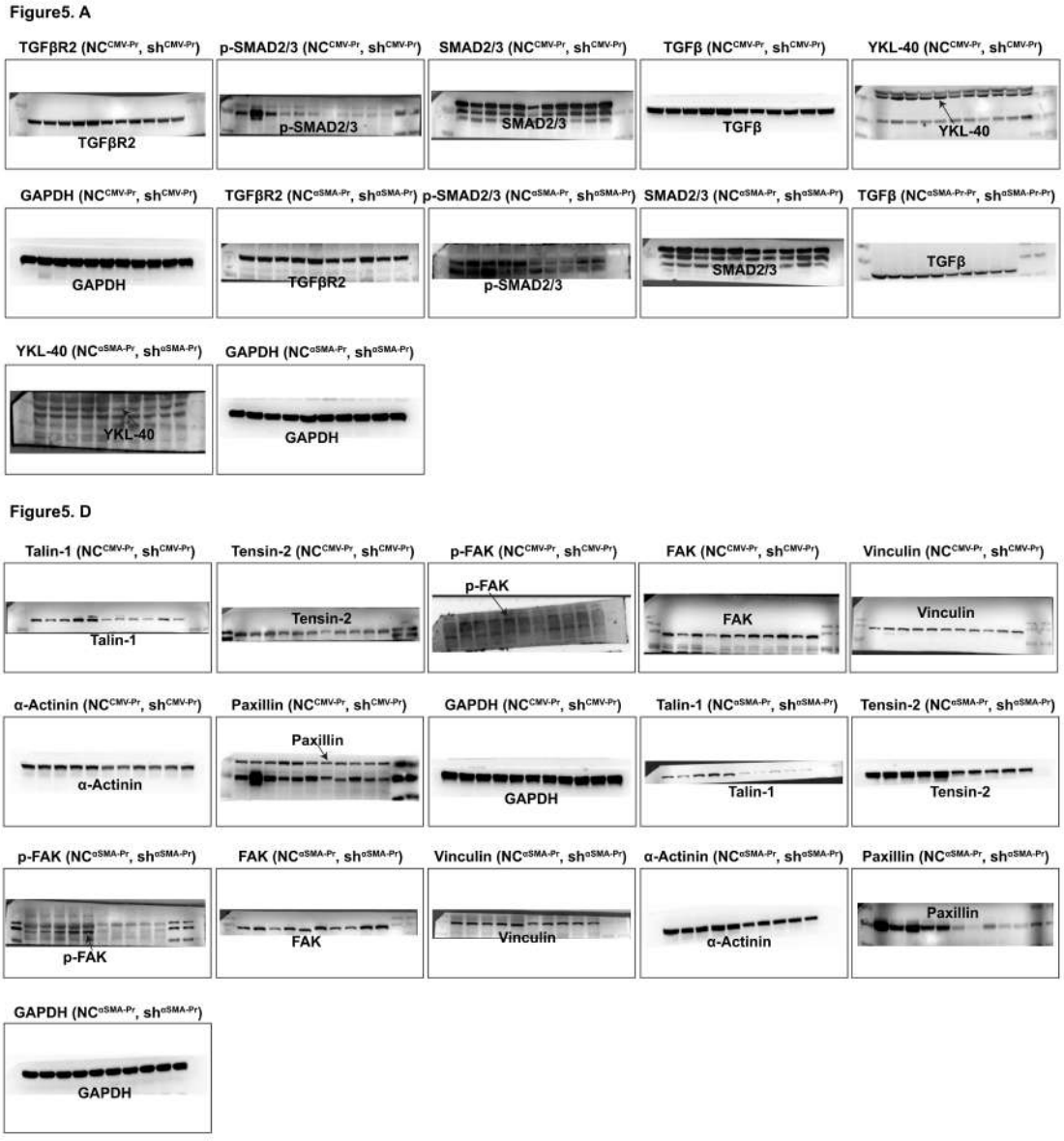

Figure S11. Full-length immunoblots related to Figure 5A and D.

Figure5. G

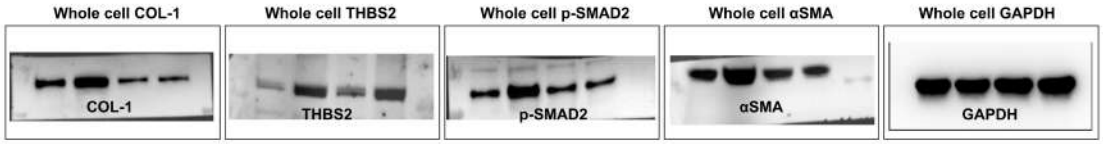

Figure5. H

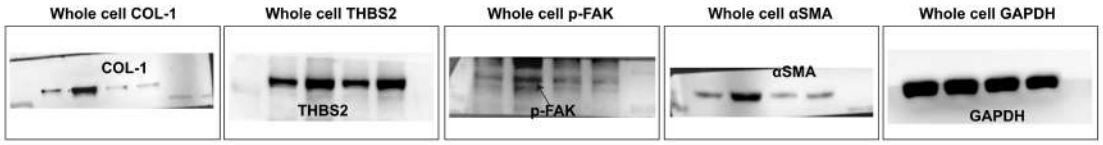

Figure6. B

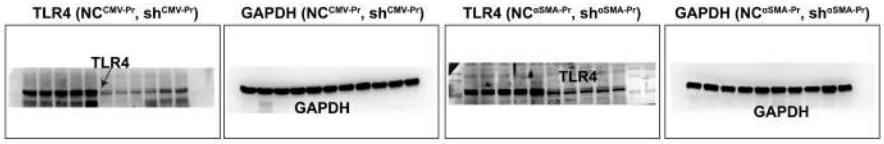

Figure6. F

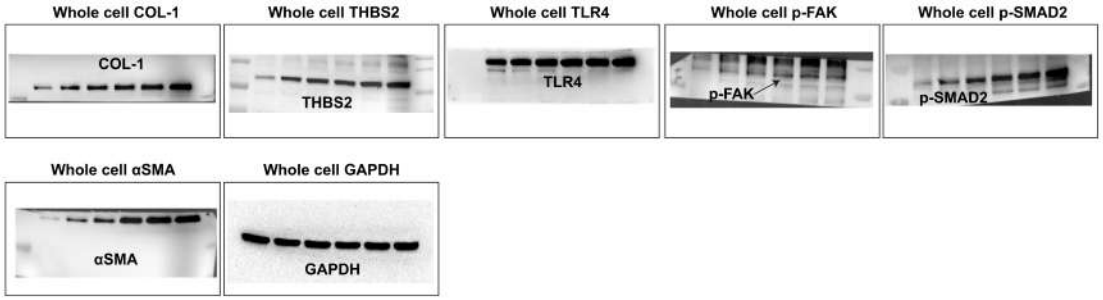

Figure6. G

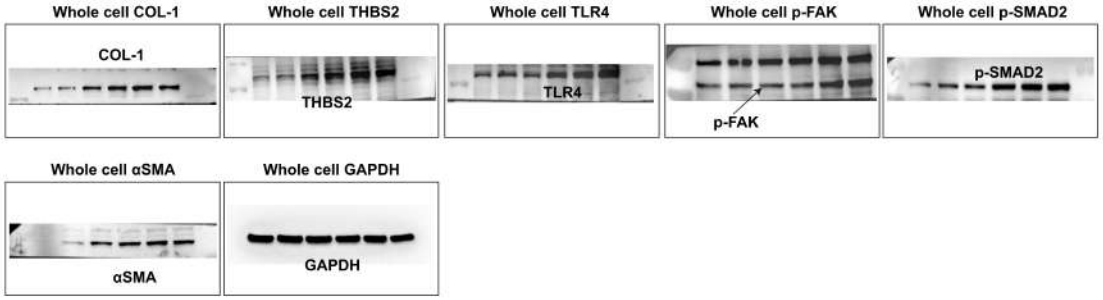

Figure S12. Full-length immunoblots related to Figure 5G, 5H, 6B, 6F and 6G.

Figure6. H

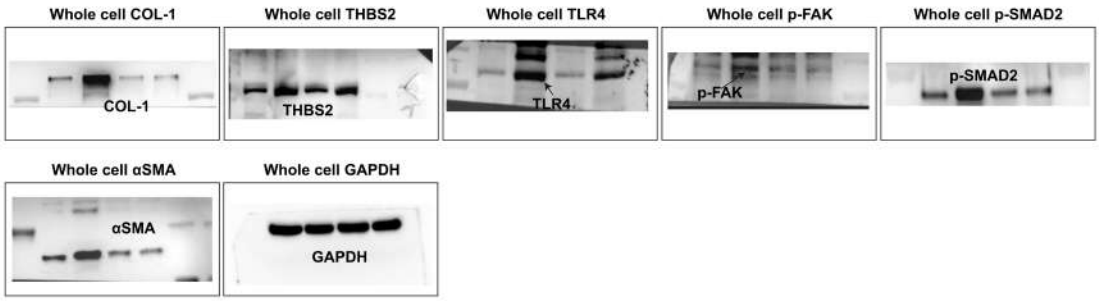

Figure7. C

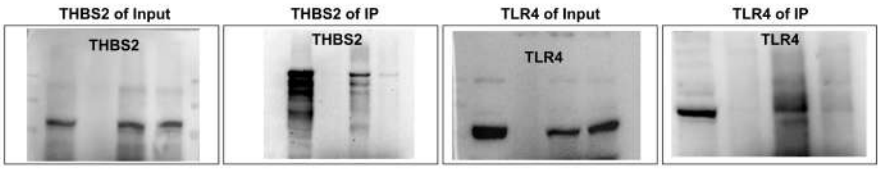

Figure7.D

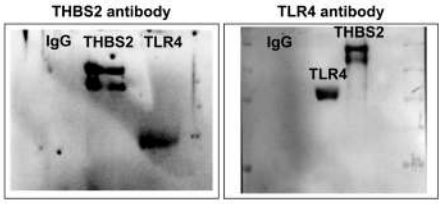

Figure7.E

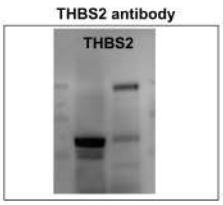

Figure S13. Full-length immunoblots related to Figure 6H, 7C, 7D and 7E.

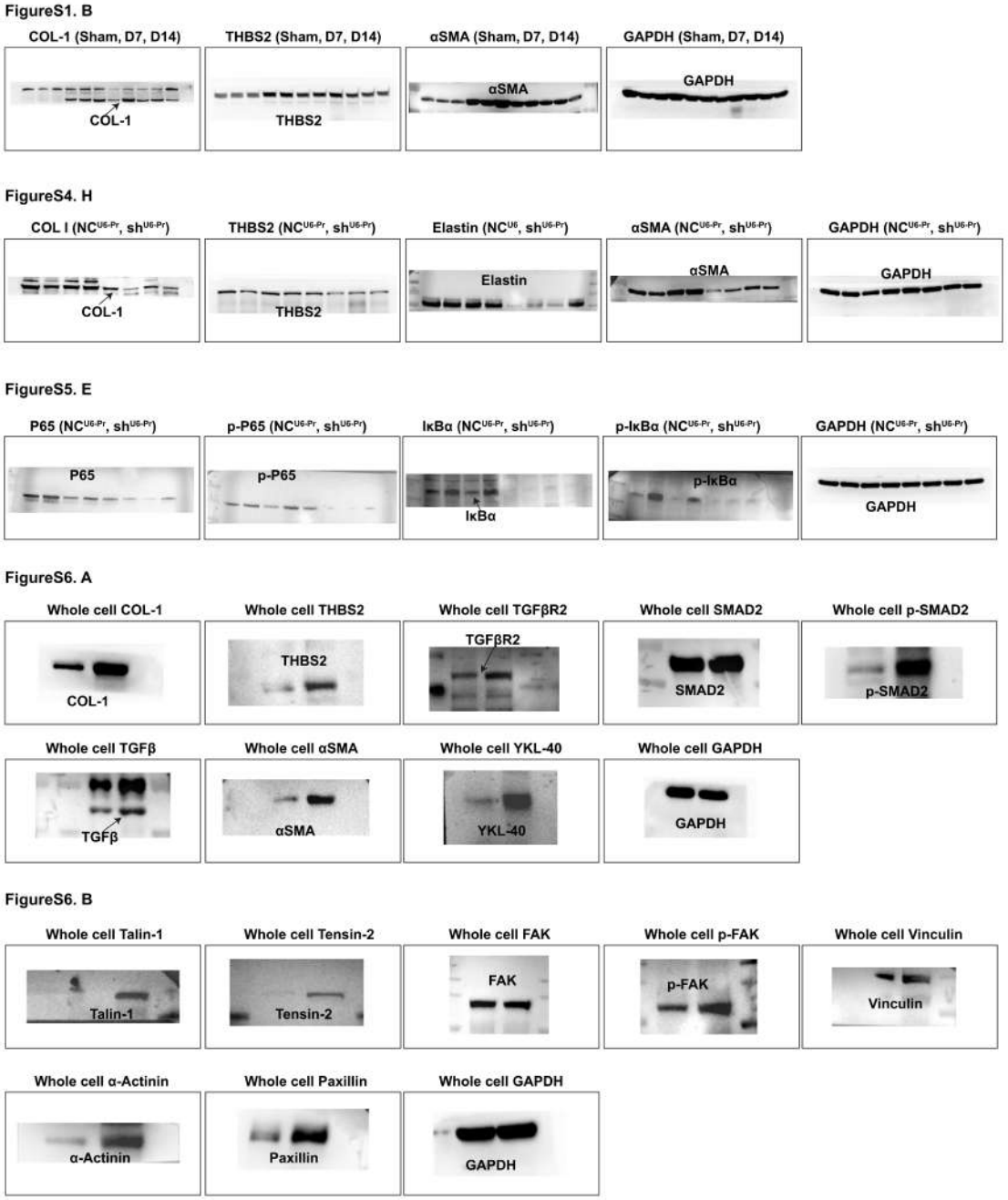

Figure S14. Full-length immunoblots related to Figure S1B, S4H, S5E, S6A and S6B.

FigureS6. C

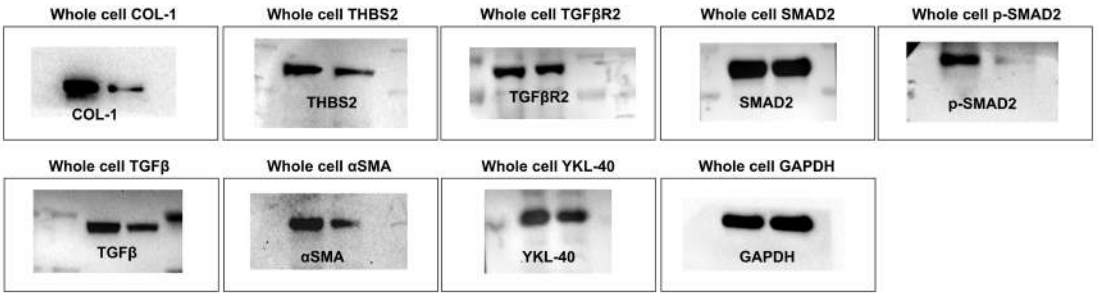

FigureS6. D

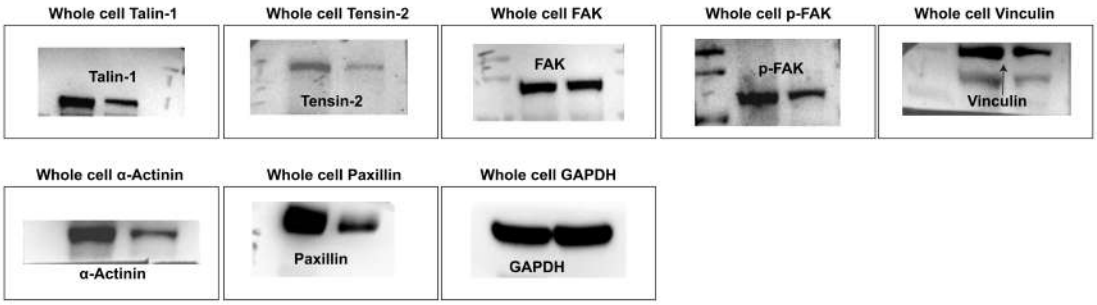

FigureS7. A

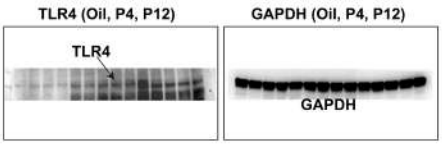

Figure S15. Full-length immunoblots related to Figure S6C, S6D and S7A.

SUPPLEMENTARY TABLES

Table S1. List of resources used in this study.

REAGENT or RESOURCE	SOURCE	IDENTIFIER
Antibodies		
Anti-COL-1 (application: WB/IF; dilution: 1:1000/1:100)	CST	Cat# 72026
Anti-THBS2 (application: IF/ICC/IP; dilution: 1:100/1:50)	Santa Cruz	Cat# sc-133061
Anti-THBS2 (application: WB; dilution: 1:500)	Abcam	Cat# ab112543
Anti-αSMA (application: WB; dilution: 1:1000)	Abcam	Cat# ab5694
Anti-αSMA (application: IF/ICC; dilution: 1:100)	Abcam	Cat# ab7817
Anti-GAPDH (application: WB; dilution: 1:10000)	Abcam	Cat# ab8245
Anti-GFP (application: IF; dilution: 1:100)	Medical & Biological Laboratories	Cat# M048-3
Anti-Elastin (application: WB; dilution: 1:1000)	Millipore	Cat# MAB2503
Anti-F4/80 (application: IHC; dilution: 1:100)	CST	Cat# 70076
Anti-F4/80 (application: IF/ICC; dilution: 1:100)	Abcam	Cat# ab6640
Anti-CD68 (application: IHC; dilution: 1:100)	Thermo Fisher Scientific	Cat# PA5-78996
Anti-CK19 (application: IHC; dilution: 1:100)	Abcam	Cat# ab52625
Anti-IκBα (application: WB; dilution: 1:1000)	CST,	Cat# 4812
Anti-p-IκBα (application: WB; dilution: 1:1000)	CST	Cat# 5209
Anti-p65 (application: WB; dilution: 1:1000)	CST	Cat# 8242
Anti-p-p65 (application: WB; dilution: 1:1000)	CST	Cat# 3031
Anti-TGFβR2 (application: WB; dilution: 1:1000)	CST	Cat# 41896
Anti-SMAD2/3 (application: WB; dilution: 1:1000)	CST	Cat# 8685
Anti-p-SMAD2/3 (application: WB; dilution: 1:1000)	CST	Cat# 8828
Anti-p-SMAD2 (application: WB; dilution: 1:1000)	CST	Cat# 18338
Anti-p-SMAD2 (application: IF/ICC; dilution: 1:100)	Thermo Fisher Scientific	Cat# 44-244G
Anti-TGF-β1 (application: WB; dilution: 1:1000)	CST	Cat# 3709
Anti-YKL40 (application: WB; dilution: 1:1000)	CST	Cat# 47066
Anti-Talin-1 (application: WB; dilution: 1:1000)	CST	Cat# 4021
Anti-Tensin-2 (application: WB; dilution: 1:1000)	CST	Cat# 11990
Anti-FAK (application: WB; dilution: 1:1000)	CST	Cat# 3285
Anti-p-FAK (application: WB; dilution: 1:1000)	CST	Cat# 8556
Anti-p-FAK (application: IF/ICC; dilution: 1:100)	Abcam	Cat# ab81298
Anti-Vinculin (application: WB; dilution: 1:1000)	CST	Cat# 4650
Anti-α-Actinin (application: WB; dilution: 1:1000)	CST	Cat# 6487
Anti-Paxillin (application: WB; dilution: 1:1000)	CST	Cat# 12065
Anti-TLR4 (application: WB/IF/ICC; dilution: 1:1000/1:100)	Thermo Fisher Scientific	Cat# PA5-23124

Anti-TLR4 (application: IF; dilution: 1:100)	Thermo Fisher Scientific	Cat# MA5-16216
Anti-FLAG (application: WB/IP/IF; dilution: 1:1000)	Medical & Biological Laboratories	Cat# M185-3L
Anti-LYVE1 (application: IF; dilution: 1:100)	Abcam	Cat# ab281587
Anti-CD34 (application: IF; dilution: 1:100)	Abcam	Cat# ab81289
Alexa Fluor 594 donkey anti-rabbit IgG(H+L) (application: secondary antibody; dilution: 1:500)	Invitrogen	Cat# A21207
Alexa Fluor 594 donkey anti-mouse IgG(H+L) (application: secondary antibody; dilution: 1:500)	Invitrogen	Cat# A21203
Alexa Fluor 488 donkey anti-rabbit IgG(H+L) (application: secondary antibody; dilution: 1:500)	Invitrogen	Cat# A21206
Alexa Fluor 488 donkey anti-mouse IgG(H+L) (application: secondary antibody; dilution: 1:500)	Invitrogen	Cat# A21202
Anti-mouse IgG HRP-linked Ab (application: secondary antibody; dilution: 1:5000)	ZSGB-Bio	Cat# ZB-2305
Anti-rabbit IgG HRP-linked Ab (application: secondary antibody; dilution: 1:5000)	ZSGB-Bio	Cat# ZB-2301
Chemicals, peptides, and recombinant proteins		
THBS2 peptide	Abcam	Cat# ab96113
rhTGF-β1	MCE	Cat# HY-P7118
rhTHBS2	ACRO Biosystems	Cat# TH2-H52H5
rhTLR4	Abcam	Cat# ab233665
TAK-242	MCE	Cat# HY-11109
LY2157299	MCE	Cat# HY-13226
PF-562271	MCE	Cat# HY-10459
Rabbit mAb IgG Isotype Control	CST	Cat# 2729
Mouse mAb IgG1 Isotype Control	CST	Cat# 33469
Commercial kits		
PrimeScript™ RT reagent Kit (Perfect Real Time)	Takara	Cat# RR037Q
Fast SYBR Green Master Mix	Applied Biosystems	Cat# 100029284
Verhoeff's Van Gieson (EVG) Staining	ZSGB-BIO	Cat# BSBA-4083B
X-tremeGENE HP DNA Transfection Reagent	Roche	Cat# 56172300
RNAFit	HanbioTech	Cat# HB-RF-1000
Human Hepatic Stellate Cell Complete Medium	Procell	Cat# CM-H046
Alanine aminotransferase Assay Kit	Nanjing Jiancheng	Cat# C009-2-1
Aspartate aminotransferase Assay Kit	Nanjing Jiancheng	Cat# C010-2-1
Mouse Thrombospondin-2(THBS2) ELISA kit	CUSABIO	Cat# CSB-EL023488MO

Immunoprecipitation lysis buffer/ Protein A/G PLUS	Thermo Fisher Scientific/Santa Cruz	Cat# 87788/sc-2003
Pierce™ Protein Concentrator PES 10K MWCO, 2-6 mL, 24PK	Thermo Fisher Scientific	Cat# 88517
Primary cells/cell lines		
Human: primary HSC	Procell	Cat# CP-H046
Human: LX-2 cell	ATCC	N/A
Human: HEK293T	ATCC	Cat# CRL-11268
Organisms/strains		
Mouse: C57BL/6J	HFK Bioscience Co. Ltd.	N/A
Mouse: collagen α1(I)-GFP transgenic mice	Gifted from Prof. David A. Brenner	N/A
Primers for quantitative RT-PCR		
Mouse_*Thbs2*_forward: 5'-CAGATTGGCTACGCAGGTGA-3' Mouse_*Thbs2*_reverse: 5'- GTTTGGGGCAGTTGTCCTTG-3'	This paper	Designed by Primer-BLAST
Mouse_*Tlr4*_forward: 5'- ATGGCATGGCTTACACCACC-3' Mouse_*Tlr4*_reverse: 5'-GAGGCCAATTTTGTCTCCACA-3'	This paper	Designed by Primer-BLAST
Mouse_*Tnf*_forward: 5'- GACGTGGAACTGGCAGAAGAG-3' Mouse_*Tnf*_reverse: 5'- TTGGTGGTTTGTGAGTGTGAG-3'	This paper	Designed by Primer-BLAST
Mouse_*Il1b*_forward: 5'-GCAACTGTTCCTGAACTCAACT-3' Mouse_*Il1b*_reverse: 5'- ATCTTTTGGGGTCCGTCAACT-3'	This paper	Designed by Primer-BLAST
Mouse_*Il6*_forward: 5'- CCAAGAGGTGAGTGCTTCCC-3' Mouse_*Il6*_reverse: 5'- CTGTTGTTCAGACTCTCTCCCT-3'	This paper	Designed by Primer-BLAST
Mouse_*Ccl2*_forward: 5'- TTAAAAACCTGGATCGGAACCAA-3' Mouse_*Ccl2*_reverse: 5'- GCATTAGCTTCAGATTTACGGGT-3'	This paper	Designed by Primer-BLAST
Mouse_*EGFP*_forward: 5'-ACTGTGTTTGCTGACGCAAC-3' Mouse_*EGFP*_reverse: 5'-CTATTTAACCGGTGCGGGGA-3'	This paper	Designed by Primer-BLAST

Mouse_*Gapdh*_forward: 5'- TGGCCTTCCGTGTTCCTAC-3' Mouse_*Gapdh*_reverse: 5'- GAGTTGCTGTTGAAGTCGCA-3'	This paper	Designed by Primer-BLAST
AAV vectors, plasmids, shRNAs and siRNAs		
AAV6-CMV-EGFP-MIR155(sh*Thbs2*)-SV40 PolyA (sh^{CMV-Pr}) Target sequence: TGATCTCAACAGGATTGTCAA	This paper	Cat# 106817-1
AAV6-CMV-EGFP-MIR155(NC)-SV40 PolyA (NC^{CMV-Pr})	This paper	Cat# CON539
AAV6-U6-sh*Thbs2*-CBh-EGFP-WPRE (sh^{U6-Pr}) Target sequence: CCATTCTATGAGCAGCTAGAA	This paper	Cat# Y17239
AAV6-U6-NC-CBh-EGFP-WPR*E* (NC^{U6-Pr})	This paper	Cat# Y13860
AAV6-αSMA-EGFP-MIR155(sh*Thbs2*)-SV40 PolyA (sh$^{αSMA-Pr}$) Target sequence: TGATCTCAACAGGATTGTCAA	This paper	Cat# 75708-32
AAV6-αSMA-EGFP-MIR155(NC)-SV40 PolyA (NC$^{αSMA-Pr}$)	This paper	Cat# 74902-6
pRP[Exp]-EGFP-EF1A>hTHBS2[NM_003247.5]/FLAG	This paper	Cat# VB220107-1253qkc
PRP[Exp]-EGFP-EF1A>FLAG/hTLR4[NM 138554.5]	This paper	Cat# VB220809-1448qzr
pRP[Exp]-EGFP-EF1A>FLAG	This paper	Cat# VB010000-9289pws
siRNA (h*THBS2*) Target sequence: ACCUGCAAGAAAUUUAAAATT	This paper	N/A
siRNA (h*THBS2*) Negative control Target sequence: UUCUCCGAACGUGUCACGUTT	This paper	N/A
LV-sh*THBS2* Target sequence: TGATCTCAACAGGATTGTCAA	This paper	Cat# GIDL0341380
LV-shNC Target sequence: ACGTGACACGTTCGGAGAA	This paper	Cat# LVCON313
Software		
ImageJ	National Institutes of Health	https://imagej.nih.gov/ij
Graphpad Prism 8	Dotmatics	https://www.graphpad.com
Gene Expression Omnibus	National Institutes of Health	https://www.ncbi.nlm.nih.gov/geo

Cytoscape 3.9.1	National Institute of General Medical Sciences	https://cytoscape.org
Image-pro plus 6.0	Media Cybernetics	https://www.mediacy.com
Sangerbox 3.0	Sangerbox	http://sangerbox.com/home.html
FV10-ASW 4.2 Viewer	Olympus Life Science	https://www.olympus-lifescience.com
Primer-BLAST	National Institutes of Health	https://www.ncbi.nlm.nih.gov/tools/primer-blast
SlideViewer	3DHISTECH	https://www.3dhistech.com
7500 Software v2.3	Applied Biosystems	https://www.thermofisher.cn/cn/zh/home/brands/applied-biosystems.html
Ingenuity Pathways Analysis	QIAGEN	https://www.qiagen.com/us
Image Lab Software	Bio-Rad	https://www.bio-rad.com/
Other		

Table S2. Publicly available gene expression profiles of liver fibrosis from GEO used in this study.

GEO ID	Etiology	Sample size	Sample resource	Platform	Year
GSE84044	HBV	F0=43 F1=20 F2=33 F3=18 F4=10	Frozen liver biopsy	GPL570	2016
GSE14323	HCV	Normal=19 LC=41	Liver transplantation	GPL571	2009
GSE49541	NAFLD	F0-1=40 F3-4=32	Frozen liver biopsy	GPL570	2013

GSE130970	NAFLD	F0=25 F1=29 F2=8 F3=14 F4=2	Frozen liver biopsy	GPL16791	2019
GSE149601	HCV	Non-LC=140 LC=55	Liver biopsy	GPL20301	2020
GSE15654	HCV	LC=216	Liver biopsy	GPL8432	2013

***Abbreviation*:** F0-4, METAVIR score 0-4; GEO, Gene Expression Omnibus; HBV, hepatitis B virus; HCV, hepatitis C virus; LC, liver cirrhosis; NAFLD, non-alcoholic fatty liver disease; non-LC, non-liver cirrhosis.